

This discussion paper is/has been under review for the journal Atmospheric Chemistry and Physics (ACP). Please refer to the corresponding final paper in ACP if available.

The diurnal evolution of the urban heat island of Paris: a model-based case study during Summer 2006

H. Wouters^{1,2}, K. De Ridder¹, N. P. M. van Lipzig², M. Demuzere², and D. Lauwaet¹

¹VITO Flemish Institute for Technological Research, Dept. Environmental and Atmospheric Modelling, Mol, Belgium

²KU Leuven, dept. Earth and Environmental Sciences, Leuven, Belquim

Received: 11 June 2012 – Accepted: 23 September 2012 – Published: 2 October 2012

Correspondence to: H. Wouters (hendrik.wouters@vito.be)

Published by Copernicus Publications on behalf of the European Geosciences Union.

ACPD

12, 25941–25981, 2012

The diurnal evolution of the urban heat island of Paris

H. Wouters et al.

[Title Page](#)

[Abstract](#)

[Introduction](#)

[Conclusions](#)

[References](#)

[Tables](#)

[Figures](#)

◀

▶

◀

▶

[Back](#)

[Close](#)

[Full Screen / Esc](#)

[Printer-friendly Version](#)

[Interactive Discussion](#)



Abstract

The urban heat island (UHI) over Paris during summer 2006 was simulated using the Advanced Regional Prediction System (ARPS) updated with a simple urban parametrization at a horizontal resolution of 1 km. Two integrations were performed, 5 one with the urban land cover of Paris and another in which Paris was replaced by cropland. The focus is on a five-day clear-sky period, for which the UHI intensity reaches its maximum. The diurnal evolution of the UHI intensity was found to be adequately simulated for this five day period. The maximum difference at night in 2-m temperature between urban and rural areas stemming from the urban heating is reproduced with a 10 relative error of less than 10 %. The UHI has an ellipsoidal shape and stretches along the prevailing wind direction. The maximum UHI intensity of 6.1 K occurs at 23:00 UTC located 6 km downstream of the city centre and this largely remains during the whole night. An idealized one-column model study demonstrates that the nocturnal differential sensible heat flux, even though much smaller than its daytime value, is mainly responsible for the maximum UHI intensity. The reason for this nighttime maximum is that 15 additional heat is only affecting a shallow layer of 150 m. At the same time, an idealized study shows that the orography around the city of Paris induces an uplift. This leads to a considerable nocturnal adiabatic cooling over cropland. In contrast, this uplift has little effect on the mixed-layer temperature over the city. About twenty percent of the 20 total maximum UHI intensity is estimated to be caused by this uplift.

1 Introduction

Temperature tends to be higher in cities than in its natural surroundings, especially during the night (Landsberg, 1981; Oke, 1987; Arnfield, 2003). This is known as the 25 urban heat island (UHI) effect. Urban surfaces distinguish themselves from their natural surroundings by particular urban surface characteristics like increased thermal inertia (Cai et al., 2008), a lowered vegetation cover and impervious land cover which reduces

ACPD

12, 25941–25981, 2012

The diurnal evolution of the urban heat island of Paris

H. Wouters et al.

Title Page	
Abstract	Introduction
Conclusions	References
Tables	Figures
◀	▶
◀	▶
Back	Close
Full Screen / Esc	
Printer-friendly Version	
Interactive Discussion	



**The diurnal evolution
of the urban heat
island of Paris**

H. Wouters et al.

the evapotranspiration (Grimmond and Oke, 1999), a different albedo, emissivity and aerodynamical characteristics due to presence of streets and buildings. Together with the release of anthropogenic heat, this leads to the UHI effect reaching its maximum during the night. It is especially favoured by high solar irradiation (clear-sky), no precipitation, low wind speeds and stable stratification. Under these conditions, a large amount of solar radiation reaches the surface, which is better transformed to heat, and subsequently retained as storage heat (Grimmond et al., 1999) for a longer time in urban areas compared to rural areas.

The UHI has a considerable impact on human environmental health. It can increase the mortality rate during summer, but especially during heat waves. Indeed, a considerable UHI can also develop during the heat wave, e.g. over Oklahoma city during summer 2008 (Basara et al., 2010). Furthermore, Smargiassi et al. (2009) found that the risk of death on warm summer days in areas with higher surface temperatures was greater than in areas with lower surface temperatures. Moreover, the death rate during the heat waves is significantly associated with the increased minimum temperature during the night (Laaidi et al., 2011; Nicholls, 2009). In addition, the UHI also deteriorates air quality due to an increase of pollutants such as ozone. Finally, it has an impact on energy consumption from cooling systems like refrigerators and air conditioning which may act as a feedback to the urban surface heating.

Several mitigation strategies for the UHI and its consequences have been suggested, e.g. by using reflective surfaces (Taha et al., 1988; Taha, 1997), or providing urban greening (Bowler et al., 2010) with vegetation (Avissar, 1996; Dimoudi, 2003) and green roofs (Alexandri and Jones, 2007). In this respect, it is indispensable to fully understand the processes that contribute to the UHI and to estimate its exact spatial impact and range. Furthermore, the inclusion of urban effects can also serve to improve weather forecasts as shown in Hamdi et al. (2012). Finally, accounting for the UHI is important when studying the effect of land-use change (e.g. forest to croplands, or vegetation cover to urban land) on climate on the mesoscale and global scale.

Title Page	
Abstract	Introduction
Conclusions	References
Tables	Figures
◀	▶
◀	▶
Back	Close
Full Screen / Esc	
Printer-friendly Version	
Interactive Discussion	

The aim of this paper is to investigate the dominant heating terms for the maximum UHI intensity, and their interaction with the orography and boundary-layer stability. Two model runs are performed with the Advanced Regional Prediction System (ARPS), a non-hydrostatic mesoscale meteorological model (Xue et al., 2000, 2001), updated 5 with a simple urban surface parametrization: the first represents the reference simulation with the actual conditions of urbanization. This run is used for the validation of the model. The second represents a scenario run for which the urban cover is replaced by crops. The different contributions of urbanization to urban surface heating and their relative importance for the development of the UHI intensity, in particular at its maximum 10 during the night, are investigated by analyzing the surface energy balance (SEB). A description of the resulting spatial extent of the maximum UHI intensity in the horizontal and vertical for Paris is given as well.

Even though the surface energy balance of the urban surface itself has already been addressed in earlier studies such as Lemonsu and Masson (2002), its change because 15 of the urbanization and its direct consequence on the nocturnal boundary-layer above have not been investigated in detail. Little is known about the role of the stable boundary layer during the night in contrast to unstable boundary conditions during the day. The mixed-layer height during the day is at least eight to ten times smaller during the night than the during the day and heat is mixed over a significantly smaller depth (Bohnen- 20 stengel et al., 2011). Yet, the direct relation between the urban surface heating and nocturnal increase in UHI intensity (and consequentially the minimum temperature) has not been investigated in detail. Therefore, an idealized advection model is developed in which a moving air column is advected over the city during the night. The model is used to study the underlying mechanisms that favour a maximum boundary- 25 layer UHI intensity at night even though the urban surface heating is relatively low at that time. In addition, it is investigated how the UHI extends in the vertical under nocturnal boundary conditions. The idealized advection model is also suitable to study how the urban surface heating interacts with orographical effects. Although this has been

The diurnal evolution of the urban heat island of Paris

H. Wouters et al.

[Title Page](#)

[Abstract](#)

[Introduction](#)

[Conclusions](#)

[References](#)

[Tables](#)

[Figures](#)

◀

▶

◀

▶

[Back](#)

[Close](#)

[Full Screen / Esc](#)

[Printer-friendly Version](#)

[Interactive Discussion](#)



studied for the day in Lemonsu and Masson (2002), little is known about orographic effects during night time.

The structure of the paper is as follows: the ARPS model setup and configuration of the runs are described in Sect. 2.1. The idealized boundary-layer advection models are presented in Sect. 2.2. The results for a 5-day period of maximum urban surface heating are presented in Sect. 3. Hereby, we start with the evaluation of the ARPS model results and UHI intensity (Sect. 3.1). Afterwards, the surface energy balance (Sect. 3.2), the horizontal and vertical extent (Sect. 3.3) of the UHI intensity are analyzed. Finally, we apply the idealized advection model (Sect. 3.4) for an in-depth analyses of the evolution of the boundary layer over the city during the night. Conclusions are formulated in Sect. 4.

2 Method

2.1 Mesoscale model description and setup

Meteorological fields are simulated using the Advanced Regional Prediction System (ARPS), a non-hydrostatic mesoscale atmospheric model developed at the University of Oklahoma (Xue et al., 2000, 2001). The turbulent fluxes of momentum and sensible heat are calculated by accounting for stability effects and the roughness sublayer (Garratt, 1992). Therein, flux-profile relationships for wind speed and temperature from Cheng and Brutsaert (2005), Businger (1966) or Dyer (1967), and De Ridder (2010) are used. These flux-profile functions are solved for $\zeta = z/L$ iteratively (z is the lowest model layer height above the displacement height and L the Obukhov Length) by establishing a relation involving the bulk Richardson number Ri_B (Arya, 2001), and using Ridder's (1979) root finding scheme as described in Press et al. (1992). The land-surface scheme used in these simulations is that of De Ridder and Schayes (1997), which contains advanced parametrizations of plant transpiration. Temperature and water content of the vegetation canopy and of five soil layers are calculated using prognostic con-

Title Page	
Abstract	Introduction
Conclusions	References
Tables	Figures
◀◀	▶▶
◀	▶
Back	Close
Full Screen / Esc	
Printer-friendly Version	
Interactive Discussion	



ervation equations, and water flow in the soil is calculated using Richard's equation (Garratt, 1992). Soil moisture and temperature were initialised using data from the Global Land Data Assimilation System (GLDAS), Rodell et al. (see 2004). For reasons of consistency, the soil texture was taken the same as that used in GLDAS. From the 5 soil texture information that comes with the GLDAS data, we estimated domain-mean fractions of clay, sand, and silt, with contributions of 25, 35, and 40%, respectively. The corresponding soil textural parameters of the Clapp and Hornberger (1978) relations used in our model are based on Cosby et al. (1984). It should be noted that, even though the soil moisture simulation is not directly relevant to anthropogenic urban 10 materials such as concrete and asphalt, it does influence the urban-rural temperature difference, which is the focus of this study, hence the care taken here to properly simulate this quantity.

The land-surface scheme was extended to represent urban surfaces as described in Demuzere et al. (2008). The main feature of that extension is the use of Zilitinkevich et al. (1992) thermal roughness length parametrization in urban areas, the thermal 15 inertia which is assigned a value of $1800 \text{ J m}^{-2} \text{ s}^{-1/2} \text{ K}^{-1}$, and the inclusion of anthropogenic heating. The latter was specified as in Demuzere et al. (2008) for Marseille, though scaled up for Paris. In Demuzere et al. (2008), the estimated anthropogenic heat flux for Marseille was found to vary between approximately 15 W m^{-2} 20 (night) and 30 W m^{-2} (day), with a linear transition between these two values during the morning and evening hours. The detailed time profile is shown in Fig. 10 of Demuzere et al. (2008). The scaling up for Paris was achieved using observed satellite-based anthropogenic light irradiance (visible nocturnal lights from space). As explained in Makar et al. (2006), such information can be related to the annual 25 mean anthropogenic heat flux. While for Marseille the estimated annual mean anthropogenic heat flux amounts to 29 W m^{-2} , for Paris this value reaches 60 W m^{-2} (see <http://www.iiasa.ac.at/Research/TNT/WEB/heat/>). Hence, the anthropogenic heat flux values over Paris were obtained applying this ratio of 2.07 (= $59.6/28.8$) to the values

The diurnal evolution of the urban heat island of Paris

H. Wouters et al.

[Title Page](#)

[Abstract](#)

[Introduction](#)

[Conclusions](#)

[References](#)

[Tables](#)

[Figures](#)

◀

▶

◀

▶

[Back](#)

[Close](#)

[Full Screen / Esc](#)

[Printer-friendly Version](#)

[Interactive Discussion](#)



obtained over Marseille, with values reaching approximately 60 W m^{-2} during daytime and half that value at night.

Aerodynamic roughness length, albedo, emissivity, and the unconstrained stomatal resistance were specified as a function of land-use type, which was interpolated from the CORINE land-cover map (European Commission 1994), see Fig. 1. Terrain height was interpolated from the Global 30 Arc Second Elevation dataset (GTOPO30) distributed by the US Geological Survey. Sea-surface temperature was derived from MODIS thermal imagery. The vegetation abundance was specified as a linear function of normalised difference vegetation index (NDVI) values interpolated from satellite imagery of the VEGETATION instrument onboard the SPOT satellite platform, following relations established by Wittich and Hansing (1995) and Gutman and Ignatov (1998).

The land-surface scheme employs the mosaic approach, allowing different land-use types to co-exist within a surface grid cell. The surface energy balance is computed individually for each land-use class, and the energy flux for each grid cell is calculated as the weighted average.

We employ a three-level one-way grid nesting at resolutions of 16, 4 and 1 km. Each of the nesting domains was run in a configuration of 100 by 100 grid cells in the horizontal direction, and 35 levels in the vertical direction, with vertical resolution starting at 25 m near the surface to approximately 1 km near the model top located at an altitude of 15 km. The 1-km model domain chosen for the simulation is the larger area of Paris, as shown in Fig. 1. The 16-km simulation was forced at its lateral boundaries by 6-h analysis fields from the operational model of the European Centre for Medium Range Weather Forecasting (ECMWF), available at a spatial resolution of 0.25° in latitude and longitude.

The model setup and configuration is applied for the period of the 1 to 13 June 2006 and is the same as from the model configuration used in Sarkar and De Ridder (2010). This run is hereafter referred to as the “base run”. The period is characterised by calm weather, low wind speeds, limited cloud and precipitation and strong temperature inversion during the night, which all favour the development of the urban heat island.

The diurnal evolution
of the urban heat
island of Paris

H. Wouters et al.

[Title Page](#)

[Abstract](#)

[Introduction](#)

[Conclusions](#)

[References](#)

[Tables](#)

[Figures](#)

◀

▶

◀

▶

[Back](#)

[Close](#)

[Full Screen / Esc](#)

[Printer-friendly Version](#)

[Interactive Discussion](#)



The diurnal evolution of the urban heat island of Paris

H. Wouters et al.

[Title Page](#)

[Abstract](#)

[Introduction](#)

[Conclusions](#)

[References](#)

[Tables](#)

[Figures](#)

[◀](#)

[▶](#)

[◀](#)

[▶](#)

[Back](#)

[Close](#)

[Full Screen / Esc](#)

[Printer-friendly Version](#)

[Interactive Discussion](#)



Besides the base run, an additional scenario run is performed during the same period for which the model setup is exactly the same, except that the urban and sub-urban fractions have been replaced by crops. For the concerned areas, obviously no NDVI satellite data is available, so the specification of vegetation abundance is problematic.

5 To tackle this problem, an image-processing technique is used. The basic idea is to determine vegetation abundance from a probability distribution for crops that corresponds to the one from the current-day situation. Furthermore, a Lee (1986) smoothing filter and a sharpening filter (Jain, 1989) is applied subsequently to get a realistic map for the vegetation abundance. More details of this data generation procedure can be found
10 in Van Weverberg et al. (2008).

The urban heat island is estimated from the difference in output between the two runs. We are interested in a time span of maximum urban surface heating, i.e. for meteorological conditions that favour a strong UHI-effect. As the heat island intensity evolves from modest to high values over the course of the period during 1 to 13 June
15 both in the observations as in the model results, a period is selected for which the overall temperature difference between the base run and the scenario run is the highest. These conditions occur during the second half of the model run, namely during a 5-day period between 8 June and 13 June.

2.2 Idealized boundary-layer advection model

20 In order to get better insight in the development of the nocturnal boundary-layer UHI, an idealized Lagrangian single-column advection model is developed. Hereby, an air column that moves along the prevailing east wind is considered. This model takes into account the nocturnal surface sensible heat flux ($w'\theta'$)₀, the initial boundary-layer profile upwind of the city and vertical wind w_h . It will be used in Sect. 3.4 to analyze the
25 evolution of the boundary-layer during the night over urban areas, and to investigate how the much smaller nocturnal surface sensible heat flux of the city compared to the day is able to increase the UHI intensity and reaches its maximum at that time. One needs to make a distinction between upward and downward surface sensible heat

flux. Therefore, sets of equations for the convective boundary layer (CBL) with surface heating and for the nocturnal (stable) boundary layer (NBL) with surface cooling are considered in Sects. 2.2.1 and 2.2.2, respectively.

2.2.1 Slab model for the convective boundary layer

5 For the CBL, the slab model from Garratt (1992) is used. It extended to account for a constant vertical velocity at the top of the CBL (Fig. 2) as demonstrated in Sect. 3.4.1.

The temperature θ of the mixed layer changes due to the upward surface sensible heat flux which is distributed over the mixer-layer height h_e :

$$\frac{d\theta}{dt} = \frac{(\overline{w'\theta'})_0}{h_e}, \quad (1)$$

10 The mixer-layer height increases due to vertical advection of potential temperature and temperature increase:

$$\frac{dh_e}{dt} = w_h - \frac{1}{\gamma} \frac{d\theta}{dt}, \quad (2)$$

15 where γ is the temperature slope of the stable temperature profile above the mixer layer, and w_h is the vertical wind speed at the mixed-layer height. This set of equations lead to a transcendental differential equation in h_e :

$$\frac{dh_e}{dt} = \frac{(\overline{w'\theta'})_0}{\gamma h_e} + w_h, \quad (3)$$

which can be solved with the Newton–Raphson numerical method (see Appendix B). Afterwards, the evolution of the temperature can be integrated from Eq. (1):

$$\theta(t) = \theta(0) + \gamma(h_e(t) - h_e(0)) - \gamma w_h t \quad (4)$$

[Title Page](#)

[Abstract](#)

[Introduction](#)

[Conclusions](#)

[References](#)

[Tables](#)

[Figures](#)

◀

▶

◀

▶

[Back](#)

[Close](#)

[Full Screen / Esc](#)

[Printer-friendly Version](#)

[Interactive Discussion](#)



2.2.2 Slab model for the nocturnal boundary layer

In case surface cooling occurs, an NBL model can be applied based on Garratt (1992, Eq. (6.74) in Sect. 6.2.6). Such an inversion-layer model is illustrated in Fig. 3.

The potential temperature at the surface (θ) changes due to the surface cooling which decreases the temperature homogeneously up to the inversion height h_i , and due to vertical advection of potential temperature which vertically shifts the temperature profile:

$$\frac{d\theta}{dt} = \frac{(\overline{w'\theta'})_0}{h_i} - \gamma w_h \quad (5)$$

$$\frac{dh_i}{dt} = -\frac{1}{\gamma} \frac{d\theta}{dt} \quad (6)$$

where w_h is the vertical wind speed at the inversion height. Equation (5) covers the following physical processes: the surface cooling cools the stable layer homogeneously up to the inversion height h_i (first term), and vertical advection of potential temperature vertically shifts the temperature profile. The fact that the temperature slope remains the same, is expressed by Eq. (6), so that a change in h_i is related to a change in temperature θ at the surface. This set of equations can be converted to a differential equation for the inversion height:

$$\frac{dh_i}{dt} = \frac{-(\overline{w'\theta'})_0}{\gamma h_i} + w_h \quad (7)$$

It can be solved in a similar way as the CBL model equations. Again, the temperature evolution follows from integration of Eq. (6):

$$\theta(t) = \theta(0) - \gamma(h_i(t) - h_i(0)) \quad (8)$$

[Title Page](#)

[Abstract](#)

[Introduction](#)

[Conclusions](#)

[References](#)

[Tables](#)

[Figures](#)

◀

▶

◀

▶

[Back](#)

[Close](#)

[Full Screen / Esc](#)

[Printer-friendly Version](#)

[Interactive Discussion](#)



3 Results

3.1 Model evaluation

In this section, the ARPS model results are evaluated for the selected week of maximum urban surface heating between 8 June 2006 (00:00 UTC) and 13 June 2006 (00:00 UTC). Radio soundings of temperature profiles, and 2 m temperature ground measurements including the urban/rural temperature difference are investigated. A comparison between the temperature profiles from the model and those from radio soundings at Trappes (location, see Fig. 1) is shown in Fig. 4. The model profiles have an overall bias and mean absolute error of -1.75 K and 1.5 K . Yet, the model is able to reproduce the overall increase in temperature over the selected period, and correctly captures day-night differences in the observed profiles. Furthermore, the 2-m temperature of 2 fixed ground stations and their difference, resp. at Melun in a rural area and Paris-Montsouris near the city centre (locations, see Fig. 1), are compared between the model output and observations for the selected 5-day period (see Fig. 5). The values for the 2-m temperature of the model are extrapolated from the lowest vertical model layer (approximately 12.5 m height) using Monin–Obukhov surface-layer profiles accounting for stability effects. We find a correlation of 0.97 and 0.99, absolute errors of 1.4 K and 1.6 K , and a cold bias of -0.92 K and -1.45 K for the urban and rural station, respectively. An overall negative bias in the vertical profiles and 2 m temperatures mainly occur during the night. A possible reason is the uncertainty in the turbulent mixing parametrization for stable boundary-layer conditions, see, e.g. Cuxart et al. (2006). The temperature *difference* between the two stations, which reflects the thermal contrast between the urban and rural areas, is now evaluated. The modeled and observed differences and their diurnal cycle are shown in Fig. 5. The respective differences have a mean of 2.81 K and 3.35 K , respectively, and we find a correlation of 0.80. The model overestimates the temperature difference with 0.54 K or 19% and starts to grow too early in the evening. The (nocturnal) maximum UHI intensity averaged for the five days is well captured by the model but with a slight overestimation. We find temperature

[Title Page](#)[Abstract](#)[Introduction](#)[Conclusions](#)[References](#)[Tables](#)[Figures](#)[◀](#)[▶](#)[◀](#)[▶](#)[Back](#)[Close](#)[Full Screen / Esc](#)[Printer-friendly Version](#)[Interactive Discussion](#)

[Title Page](#)[Abstract](#)[Introduction](#)[Conclusions](#)[References](#)[Tables](#)[Figures](#)[|](#)[|](#)[◀](#)[▶](#)[Back](#)[Close](#)[Full Screen / Esc](#)[Printer-friendly Version](#)[Interactive Discussion](#)

differences of 6.0 K and 5.5 K for model output and observations, respectively, so it is overestimated by 0.5 K or 9.1 %. Although the model has an overall negative bias during the night, the urban-scale temperature fluctuations, which includes the UHI, are well represented in the model. Furthermore, the fact that the temperature difference between the urban and rural station becomes zero in the scenario run (for which the urban surface is replaced by crops) confirms that it is caused by the urban surface heating.

3.2 The surface energy balance

As a start to investigate the effect of urban surface heating on the evolution of the UHI, the surface energy balance (SEB) in the city centre is analyzed. The averaged diurnal cycle over the selected period is considered so that short-term fluctuations are averaged out (see Fig. 6).

The surface energy balance, which is a statement of the energy conservation at the surface, can be written as:

$$15 \quad Q^* + Q_F = Q_H + Q_E + \Delta Q_S, \quad (9)$$

where Q^* is the net all wave radiation flux density, Q_F the anthropogenic heat, Q_H and Q_E resp. the turbulent sensible and latent heat release and ΔQ_S the storage heat flux. Furthermore, Q^* is composed of net shortwave (Q_K) and long-wave radiation (Q_L):

$$Q^* = Q_K + Q_L = (K_{\downarrow} - K_{\uparrow}) + (L_{\downarrow} - L_{\uparrow}), \quad (10)$$

20 where K_{\downarrow} and L_{\downarrow} are the incoming short-wave and long-wave radiation, and K_{\uparrow} and L_{\uparrow} the outgoing short-wave and long-wave radiation.

The surface fluxes at Paris-Montsouris are compared between the base run and scenario run. In the former, the grid-cell has 85 % of urban land surface. In the latter, the urban surface is replaced by vegetation in which similar surface fluxes are obtained as for the base run at the rural location at Melun.

The diurnal evolution of the urban heat island of Paris

H. Wouters et al.

During the day, a large reduction in latent heat release ($Q_E^{\text{base}} - Q_E^{\text{scen}}$), an increase in absorbed solar radiation ($Q_K^{\text{base}} - Q_K^{\text{scen}}$) and an anthropogenic heat Q_F for the urban surface is balanced by an increase in net outgoing long-wave radiation ($-(Q_L^{\text{base}} - Q_L^{\text{scen}})$), storage heat storage heat flux $\Delta Q_S^{\text{base}} - \Delta Q_S^{\text{scen}}$ and sensible heat flux $Q_H^{\text{base}} - Q_H^{\text{scen}}$ in the city centre. This is also found in earlier studies such as Van Weverberg et al. (2008); Lemonsu and Masson (2002); Lemonsu et al. (2009); Bohnenstengel et al. (2011). The reduction in latent heat is the most important urban heating mechanism during the day as it is much larger than the anthropogenic heat and the difference in net incoming shortwave radiation. The increase in sensible heat release leads to a slight increase of 2 K at 2 m height during the day (see Fig. 5).

During the night, an excess in storage heat ($\Delta Q_S^{\text{base}} - \Delta Q_S^{\text{scen}}$) and a anthropogenic heat flux Q_F are balanced by an increased net outgoing long-wave radiation ($-(Q_L^{\text{base}} - Q_L^{\text{scen}})$) and a differential surface sensible heat ($Q_H^{\text{base}} - Q_H^{\text{scen}}$). In particular, Q_H^{base} is positive as opposed to Q_H^{scen} which is negative. It is remarkable that the impact on the 2-m temperature is increased further during the night, even though $Q_H^{\text{base}} - Q_H^{\text{scen}}$ is much smaller than during the day. It can be explained by stable stratification during the night which retains the urban heating in the base run close to the ground, as mentioned in Bohnenstengel et al. (2011). The further intensification of the UHI during the night with relative small difference in surface sensible heat flux is demonstrated in a rigorous way in Sect. 3.4.2 with the single-column Lagrangian advection model.

Note that over the urban surface, in which we are dealing with bluff-rough elements, much lower thermal roughness lengths occur in the city (Sugawara and Narita, 2008) compared to vegetative areas which reduce the turbulent transfer of heat from the surface during the day. This is in contrast to what one may expect from high roughness lengths for momentum in cities which actually tend to increase the turbulent transfer. This turbulence inhibition which blocks the surface sensible heat release during the day, together with the higher heat capacity of the urban surface with a large amount of buildings (Lemonsu and Masson, 2002; Harman and Belcher, 2006; Oleson et al., 2011),

Title Page	
Abstract	Introduction
Conclusions	References
Tables	Figures
◀	▶
◀	▶
Back	Close
Full Screen / Esc	
Printer-friendly Version	
Interactive Discussion	



is important because it favours an increase of storage heat. The latter is released subsequently as sensible heat during the night and this consequently influences the nocturnal temperature (profile) demonstrated in Sect. 3.4.2.

In the early morning, a decrease in temperature difference between urban and rural station is partly explained by the increased storage heat opposed to the excess sensible heat. This stems from the already mentioned large heat capacity of urban surfaces and from the heat blocking effect due to very low thermal roughness lengths for bluff-rough elements typical for urban areas. This could even lead to an urban “cool” island which can last for the whole day, as found over Oklahoma city (Lemonsu et al., 2009).

Nevertheless in this case study for Paris, the excess in sensible heat release remains positive in the morning which would still suggest an increase instead of decrease in temperature difference. Yet, the UHI intensity is reduced since the excess in sensible heat and temperature is distributed by turbulent diffusion due to the development of a convective boundary layer.

To conclude, the large reduction of the latent heat release, and to a lesser extent the reduced reflected solar radiation and anthropogenic heat for urban surfaces basically explain the large increase in storage heat uptake at noon and sensible heat release in the afternoon. The latter results in a modest impact on the near-surface temperature as it is mixed over a larger depth because of unstable stratification. The heat which was stored during the day and, to a lesser extent, the added anthropogenic heat results in a small impact on the sensible heat during the night. However, this leads to a much stronger impact on the near-surface temperature compared to the day. At that time, the UHI is at its maximum as this extra heat is retained close to the ground because of stable stratification.

3.3 The horizontal and vertical extent of the urban heat island

The maximum UHI intensity at 23:00 UTC of 6.1 K is found at about 6 km downwind of the city centre along the wind vector (Fig. 7). This downwind shift is also found in Bohnenstengel et al. (2011). In fact, the boundary-layer UHI increases when moving

Title Page	
Abstract	Introduction
Conclusions	References
Tables	Figures
◀	▶
◀	▶
Back	Close
Full Screen / Esc	
Printer-friendly Version	
Interactive Discussion	



over the city along the wind vector up to the location where the excess in sensible heat release induced by the urban surface vanishes. The extent of the UHI has approximately the same horizontal size as the total area of the suburban and urban terrain of Paris. The UHI intensity is much lower during the day (Fig. 8), even though the magnitude and extent of the differential sensible heat flux is much larger than during the night. The downwind shift of the UHI intensity is negligible in the results for the day.

During the day between 09:00 UTC and 18:00 UTC, the large excess in sensible heat is found in Sect. 3.2. This is distributed over large depth of the convective boundary layer during the day (Fig. 9). This vertical distribution limits the UHI intensity to at most 10 2.5 K near the surface, but a small impact on the vertical temperature of 0.5 K is still found up to the mixing height of 800 m. During the night, a positive instead of negative 15 Q_H^{base} is found. As a consequence, a neutral mixed layer with a small depth is formed over the city, while the temperature profile becomes stable over cropland. The UHI intensity increases up to 6.1 K at 23:00 UTC 6 km downwind of the city centre with a decreasing lapse rate of 0.05 Km^{-1} (Fig. 10). The UHI intensity is confined to 150 m depth under nocturnal boundary-layer conditions, hence the large impact of a relative small excess in sensible heat. This is discussed hereafter with the idealized advection approach. The differential surface sensible heat remains positive for the entire night under nocturnal stability. Therefore, the UHI persists with only a slight decrease until 20 the morning (6:00 UTC) when a convective boundary layer with a large depth is formed. Note that a small cooling of about -0.5 K occurs at 200–400 m above the city. This can be ascribed to the cross-over effect (Cermak et al., 1995; Oke, 1982): entrainment occurs at the elevated inversion base above the city due to roughness and buoyancy 25 effects. This cross-over effect might then correspond to the layer from which heat has been removed by entrainment.

[Title Page](#)[Abstract](#)[Introduction](#)[Conclusions](#)[References](#)[Tables](#)[Figures](#)[|◀](#)[▶|](#)[◀](#)[▶](#)[Back](#)[Close](#)[Full Screen / Esc](#)[Printer-friendly Version](#)[Interactive Discussion](#)

3.4 The advection model: mechanisms explaining the development of the nocturnal UHI

ACPD

12, 25941–25981, 2012

The diurnal evolution of the urban heat island of Paris

H. Wouters et al.

3.4.1 Advection model setup

10 The advection approach is applied for both scenarios between 22:00 UTC and 23:00 UTC starting 6 km upwind of the city centre traveling a distance of 12.6 km. Hereby, a horizontal wind of 3.5 m s^{-1} and a constant surface sensible heat is considered, see Fig. 11.

15 Boundary conditions for the model are taken from the ARPS simulations described in Sect. 3.3. For the base case in which urban surface heating is included, a constant sensible heat sink of -10 W m^{-2} is considered for the first 12 min (NBL) and a heat source of 15 W m^{-2} during the 48 subsequent minutes (CBL). For the scenario case in which urban surface heating is excluded, a surface sensible heat sink of -20 W m^{-2} is prescribed for the entire hour (NBL). These inputs for the advection model resemble 20 the ARPS model results for the 5-day average between 22:00 and 23:00 UTC in the respective scenarios. Idealized profiles are considered for the initial state of the advection model as a best fit to the ARPS model results at 22:00 UTC 6 km upwind (east) of the city centre for both scenarios (Fig. 12a). Note that the profile of the base case is already somewhat destabilized because of the less negative surface sensible heat 25 compared to the scenario case before 22:00 UTC.

We consider a vertical wind relative to the surface when moving along the prevailing wind of 0.012 m s^{-1} . This appears over a considerable part of the city in the ARPS

Discussion Paper | Discussion Paper

Discussion Paper | Discussion Paper

Discussion Paper | Discussion Paper

Title Page	
Abstract	Introduction
Conclusions	References
Tables	Figures
◀	▶
◀	▶
Back	Close
Full Screen / Esc	
Printer-friendly Version	
Interactive Discussion	



output, and is established by the flow over the ramp east of the city centre. The order of magnitude of this vertical uplift relative to the surface can be reproduced theoretically by considering a stratified flow over an idealized ramp in which the acceleration occurs at the downward slope east of the city centre (Appendix A). Note that the radiative cooling is neglected in the CBL and NBL models. This can be justified by the fact that the radiative cooling is an order of magnitude lower than the surface cooling/heating. For example, Ha and Mahrt (2003) found a radiation-related cooling of the order of only 0.2 K h^{-1} for a similar nocturnal situation.

3.4.2 Advection model results

10 When the air parcel moves over the city, the CBL and NBL models, that include sensible surface heating and orographically-induced uplift (LIFT), could reproduce the evolution of the near-surface temperature profiles for the lowest 150 metres very well for the respective scenarios (Fig. 12b). They clearly demonstrate that the nocturnal urban surface heating and vertical ramp uplift are the processes dominating the changes

15 in the temperature profiles in both scenarios. In the base case with the city of Paris, a mixed layer is formed up to a height h_e of 80 m due to surface heating, and a stable layer remains aloft. In the scenario case where the city of Paris is replaced by cropland, a stable profile persists which is cooled efficiently in the vertical up to the inversion height h_i due to a constant surface cooling and vertical advection of potential temperature.

20 Meanwhile, the inversion height is displaced in the upward direction.

To study the role of the orographically-induced vertical motion, a second run (NLFT) with the idealized advection model is performed by excluding upward motion ($w_h = 0$). In the base case, the effect of neglecting the uplift on the near-surface temperature is small, but the layer between 50 and 200 m is significantly warmer because of the absence of adiabatic cooling, and the mixed-layer height is reduced to 55 m. The effect of the uplift on the near-surface temperature is much greater in the scenario run where the city of Paris is replaced by cropland. It even turns out that in the scenario run, the cooling and increase in inversion height because of vertical heat advection is much

The diurnal evolution of the urban heat island of Paris

H. Wouters et al.

[Title Page](#)

[Abstract](#)

[Introduction](#)

[Conclusions](#)

[References](#)

[Tables](#)

[Figures](#)

◀

▶

◀

▶

[Back](#)

[Close](#)

[Full Screen / Esc](#)

[Printer-friendly Version](#)

[Interactive Discussion](#)



The diurnal evolution of the urban heat island of Paris

H. Wouters et al.

greater than from the surface cooling alone. The reduced sensitivity of the near-surface temperature to the uplift in the base run is due to the formation of a small mixing layer as response to positive sensible heat flux over the city. In this mixed layer, where the potential temperature is constant, the vertical heat advection becomes zero even though there is vertical motion. Only a slight reduction in the mixed-layer temperature appears because the sensible heat is mixer over a slightly increased mixed-layer height due to the uplift. The largest sensitivity to vertical heat advection is therefore not close to the surface, but in the layer between 50 to 200 m where the potential temperature is not constant and adiabatic cooling is important.

If only the surface sensible heat flux is considered ($w_h = 0$), the relatively low difference between the base case and scenario case in surface heating between 22:00 UTC and 23:00 UTC increases the UHI to 4.8 K (compare “base NLFT” with “scen NLFT” in Fig. 12b). The vertical advection due to the uplift caused by the ramp upwind (east) of the city centre, establishes an extra adiabatic cooling in the scenario case of 1.8 K, but only 0.5 K in the base case. Therefore, an additional UHI intensity of 1.3 K is explained by this decrease in adiabatic cooling which is about 20% of the total UHI intensity (6.1 K).

Note that the adiabatic cooling due to orographic forcing only exists for the nocturnal situation, and does not affect the near-surface temperature or UHI intensity during the day. Indeed, the near-surface potential temperature for the scenario run (Fig. 7b) resembles the orography around Paris (Fig. 1), which is not the case in the scenario run for the day (Fig. 8). It stems from the fact that during the day, it is dealt with a CBL in both scenarios for which the (change in) vertical heat advection is negligible as mentioned above, especially when the mixed-layer height is very high.

25 To conclude this section, the advection model demonstrates that the main part of the maximum UHI intensity occurring at night is directly related to the nocturnal positive differential surface sensible heat flux between the urban surface and vegetated areas. Despite this much smaller difference in surface sensible heat flux compared to the day, the UHI intensity reaches its maximum during the night, because it is confined to the

Title Page

Abstract

Introduction

Conclusions

References

Tables

Figure

→

Back

Close

Full Screen / Esc

[Printer-friendly Version](#)

Interactive Discussion



lowest 150 m above ground level as opposed to the day. The decrease in nocturnal orographically-induced adiabatic cooling explains 20% of the total UHI intensity.

4 Conclusions

Using a mesoscale meteorological model at a horizontal resolution of 1 km and covering an area of 100 km \times 100 km, the urban heat island over Paris during summer 2006 is studied. A base run is performed in which the present-day (urban) surface characteristics are represented, and an additional scenario run in which the urban surface is replaced by cropland. A 5-day period is analyzed for which the (boundary-layer) UHI intensity is high. Even though the urban parametrization is not complicated, the UHI intensity is simulated very well. In particular, the maximum difference in 2-m temperature between urban and rural areas stemming from the urban heating is reproduced with a relative error of less than 10%.

The dominant heating terms and their relative importance for the development of the maximum UHI intensity occurring during the night are analyzed. The interactions between the urban surface heating, boundary-layer stability, and orography were investigated. It was found that the increased storage-heat uptake during the day, which is subsequently released during the night, is the most important reason for the difference in surface sensible heat during the night. The nocturnal anthropogenic heat release is important as well. The increased storage heat uptake stems from the reduced evapo-transpiration in the city, the large heat capacity and the very small thermal roughness lengths of the urban surface.

Even though the nocturnal differential urban sensible heat is much lower than during the day, the UHI intensity reaches its maximum during the night. In order to investigate this behaviour in a rigorous way, idealized advection models for the NBL and CBL are developed which account for the prevailing wind, turbulent surface heating/cooling and vertical uplift. Hereby, the nocturnal evolution of the temperature profile was well reproduced for both scenarios implying that vertical and horizontal advection and the

Title Page	
Abstract	Introduction
Conclusions	References
Tables	Figures
◀	▶
◀	▶
Back	Close
Full Screen / Esc	
Printer-friendly Version	
Interactive Discussion	



The diurnal evolution of the urban heat island of Paris

H. Wouters et al.

[Title Page](#)

[Abstract](#)

[Introduction](#)

[Conclusions](#)

[References](#)

[Tables](#)

[Figures](#)

[◀](#)

[▶](#)

[◀](#)

[▶](#)

[Back](#)

[Close](#)

[Full Screen / Esc](#)

[Printer-friendly Version](#)

[Interactive Discussion](#)



Orographic flow over a ramp

As apparent from Sect. 3.4.2, the vertical uplift plays an important role in explaining the evolution of the nocturnal temperature profiles, both for the base case as the scenario simulation. ARPS simulation results clearly show uplift over the city at the western (downwind) side of a ramp located at approx. 2.55° E. Here, we try to verify whether this orographic feature (i.e. the ramp) is capable of explaining the simulated (in ARPS) vertical wind field relative to the slope wind, which is characterized by wind speed values of the order of a few cm s^{-1} .

We calculate the flow field induced by a ramp (Fig. A1) for a stably stratified atmosphere characterized by a lapse rate and a (constant) wind speed U , following Lin (2007), to do so. We assume that the stable stratification extends to infinity in the vertical direction, which is obviously a gross simplification compared to the actual situation (cfr. ARPS result), in which a stably stratified inversion layer is located underneath a residual neutral layer. We describe the orography of the ramp with height h_m and horizontal scale a as

$$h_m(x) = \frac{1}{2}h_m \left[1 - \frac{2}{\pi} \arctan \frac{x}{a} \right] \quad (\text{A1})$$

This functional form has the advantage of having a derivative that can be easily Fourier-transformed (see below).

As in Lin (2007), we obtain the perturbation vertical velocity $w'(x, z)$ by solving the Scorer equation for its Fourier-transform $\hat{w}(k, z)$,

$$\frac{\partial^2 \hat{w}}{\partial z^2} + k^2 - l^2 \hat{w} = 0 \quad (\text{A2})$$

The diurnal evolution
of the urban heat
island of Paris

H. Wouters et al.

[Title Page](#)[Abstract](#)[Introduction](#)[Conclusions](#)[References](#)[Tables](#)[Figures](#)[◀](#)[▶](#)[◀](#)[▶](#)[Back](#)[Close](#)[Full Screen / Esc](#)[Printer-friendly Version](#)[Interactive Discussion](#)

with k the horizontal wavenumber, and $l = N/U$ the vertical wave number, with $N = \sqrt{g\gamma/\theta_0}$ the Brunt–Visala frequency, g the gravitational acceleration and $\theta \simeq 300\text{K}$ a reference temperature.

The lower boundary condition on the vertical velocity is given by

$$w'(x, 0) = U \frac{dh_m}{dx} = -\frac{U\bar{h}_m}{\pi} \frac{a}{a^2 + x^2} \quad (\text{A3})$$

and its Fourier transform is

$$\hat{w}(k, 0) = \frac{1}{2\pi} \int_{-\infty}^{+\infty} w'(x, 0) e^{-ikx} dx = -\frac{U\bar{h}_m}{2\pi} e^{-ka} \quad (\text{A4})$$

with the requirement that $k > 0$.

The vertical velocity is then obtained by applying the inverse one-sided Fourier transform,

$$w'(x, z) = 2\Re \left\{ \int_0^{\infty} \hat{w}(k, 0) e^{ikx} dk \right\} = -\frac{U\bar{h}_m}{\pi} \frac{a \cos(lz) - x \sin(lz)}{a^2 + x^2}. \quad (\text{A5})$$

However, as we are interested in an ABL slab that follows the terrain, the terrain-following vertical velocity $w'(x, 0)$ has to be subtracted, so that finally

$$w'(x, z) = -\frac{U\bar{h}_m}{\pi} \frac{a \cos(lz) - 1 - x \sin(lz)}{a^2 + x^2}, \quad (\text{A6})$$

which is shown in Fig. A1 for $U = 3.5\text{ ms}^{-1}$, $a = 1000\text{ m}$, $\gamma = 0.04\text{ Km}^{-1}$, $h_m = 70\text{ m}$, and $\theta_0 = 300\text{ K}$.

From this, it appears that, despite the simplifications, our simple orographic model is capable of reproducing the order of magnitude of the vertical wind speed.

[Title Page](#)

[Abstract](#)

[Introduction](#)

[Conclusions](#)

[References](#)

[Tables](#)

[Figures](#)

[◀](#)

[▶](#)

[◀](#)

[▶](#)

[Back](#)

[Close](#)

[Full Screen / Esc](#)

[Printer-friendly Version](#)

[Interactive Discussion](#)



Solution of Eq. (3)

In this appendix we seek a solution for:

$$\frac{dh_e}{dt} = \frac{w'\theta'}{\gamma h_e} + w_h \quad (B1)$$

5 Subject to the initial condition $h_e(0) = h_0$.

Performing a change of variable $h_e \equiv p^{-1}$, this equation converts into a somewhat more manageable form, which can be integrated to yield, at time t ,

$$\frac{w'\theta'}{\gamma w_h^2} \ln \left[\frac{w'\theta'\gamma^{-1} + w_h h_0}{w'\theta'\gamma^{-1} + w_h h_e t} \right] + \frac{h_e t - h_0}{w_h} - t = 0. \quad (B2)$$

This is a transcendental equation in $h_e(t)$, which can be solved to any desired accuracy
10 by mean of, e.g. the Newton–Raphson iterative zero-finding algorithm. In the case of $w_h = 0$, Eq. (B2) cannot be applied, but the solution of Eq. (B1) is then trivial, and given by:

$$h_e(t) = \sqrt{h_0^2 + w'\theta'\gamma^{-1}t}. \quad (B3)$$

Supplementary material related to this article is available online at:

15 [http://www.atmos-chem-phys-discuss.net/12/25941/2012/
acpd-12-25941-2012-supplement.zip](http://www.atmos-chem-phys-discuss.net/12/25941/2012/acpd-12-25941-2012-supplement.zip).

Acknowledgements. This research has been conducted within a collaboration between VITO and KU Leuven for improving the meteorological forcing for urban-scale air-quality simulations. It was supported by the program Science for a Sustainable Development (SSD) of the Belgian
20 Science Policy Office (BELSPO) under contract number SD/CS/04A.

Title Page	Abstract	Introduction
Conclusions	References	
Tables	Figures	
◀◀	▶▶	
◀	▶	
Back	Close	
Full Screen / Esc		
Printer-friendly Version		
Interactive Discussion		



References

Alexandri, E. and Jones, P.: Developing a one-dimensional heat and mass transfer algorithm for describing the effect of green roofs on the built environment: comparison with experimental results, *Build. Environ.*, 42, 2835–2849, doi:10.1016/j.buildenv.2006.07.004, 2007. 25943

5 Arnfield, A. J.: Two decades of urban climate research: a review of turbulence, exchanges of energy and water, and the urban heat island, *Int. J. Climatol.*, 23, 1–26, doi:10.1002/joc.859, 2003. 25942

Arya, S. P.: *Introduction to Micrometeorology*, 2nd edn., Academic Press, San Diego, 2001. 25945

10 Avissar, R.: Potential effects of vegetation on the urban thermal environment, *Atmos. Environ.*, 30, 437–448, doi:10.1016/1352-2310(95)00013-5, 1996. 25943

Basara, J. B., Basara, H. G., Illston, B. G., and Crawford, K. C.: The impact of the urban heat island during an intense heat wave in Oklahoma City, *Adv. Meteorol.*, 2010, 1–10, doi:10.1155/2010/230365, 2010. 25943

15 Bohnenstengel, S. I., Evans, S., Clark, P. A., and Belcher, S.: Simulations of the London urban heat island, *Q. J. R. Meteorol. Soc.*, 137, 1625–1640, doi:10.1002/qj.855, 2011. 25944, 25953, 25954

Bowler, D. E., Buyung-Ali, L., Knight, T. M., and Pullin, A. S.: Urban greening to cool towns and cities: a systematic review of the empirical evidence, *Land. Urban Plan.*, 97, 147–155, doi:10.1016/j.landurbplan.2010.05.006, 2010. 25943

20 Businger, J. A.: Transfer of momentum and heat in the planetary boundary layer, *Proc. Symp. Arctic Heat Budget and Atmospheric Circulation*, The RAND Corporation, 305–331, 1966. 25945

Cai, G., Du, M., Xue, Y., and Li, S.: Analysis of an Urban Heat Sink using Thermal Inertia Model from ASTER Data in Beijing, China, in: *Geoscience and Remote Sensing Symposium, 2008, IGARSS 2008*, Boston, Massachusetts, USA, IEEE International, doi:10.1109/IGARSS.2008.4779609, III-1346–III-1349, ISBN:978-1-4244-2807-6, 2008. 25942

25 Cermak, J. E., Davenport, A. G., Plate, E. J., and Viegas, D. X.: *Wind Climate in Cities*, Kluwer, Dordrecht, 1995. 25955

The diurnal evolution of the urban heat island of Paris

H. Wouters et al.

[Title Page](#)

[Abstract](#)

[Introduction](#)

[Conclusions](#)

[References](#)

[Tables](#)

[Figures](#)

◀

▶

◀

▶

[Back](#)

[Close](#)

[Full Screen / Esc](#)

[Printer-friendly Version](#)

[Interactive Discussion](#)



Cheng, Y. G. and Brutsaert, W.: Fluxprofile relationships for wind speed and temperature in the stable atmospheric boundary layer, *Bound.-Lay. Meteorol.*, 114, 519–538, doi:10.1007/s10546-004-1425-4, 2005. 25945

5 Clapp, R. B. and Hornberger, G. M.: Empirical equations for some soil hydraulic properties, *Water Resour. Res.*, 14, 601–604, doi:10.1029/WR014i004p00601, 1978. 25946

Cosby, B. J., Hornberger, G. M., Clapp, R. B., and Ginn, T. R.: A statistical exploration of the 10 relationships of soil moisture characteristics to the physical properties of soils, *Water Resour. Res.*, 20, 682, doi:10.1029/WR020i006p00682, 1984. 25946

Cuxart, J., Holtslag, A. A. M., Beare, R. J., Bazile, E., Beljaars, A., Cheng, A., Conangla, L., 15 Ek, M., Freedman, F., Hamdi, R., Kerstein, A., Kitagawa, H., Lenderink, G., Lewellen, D., Mailhot, J., Mauritzen, T., Perov, V., Schayes, G., Steeneveld, G.-J., Svensson, G., Taylor, P., Weng, W., Wunsch, S., and Xu, K.-M.: Single-column model intercomparison for a stably stratified atmospheric boundary layer, *Bound.-Lay. Meteorol.*, 118, 273–303, doi:10.1007/s10546-005-3780-1, 2006. 25951

20 De Ridder, K.: Bulk transfer relations for the roughness sublayer, *Bound.-Lay. Meteorol.*, 134, 257–267, doi:10.1007/s10546-009-9450-y, 2010. 25945

De Ridder, K. and Schayes, G.: The IAGL land surface model, *J. Appl. Meteor.*, 36, 167–182, doi:10.1175/1520-0450(1997)036<0167:TILSM>2.0.CO;2, 1997. 25945

25 Demuzere, M., De Ridder, K., and van Lipzig, N. P. M.: Modeling the energy balance in Mar-seille: sensitivity to roughness length parametrizations and thermal admittance, *J. Geophys. Res.*, 113, 1–19, 2008. 25946

Dimoudi, A.: Vegetation in the urban environment: microclimatic analysis and benefits, *Energy Build.*, 35, 69–76, doi:10.1016/S0378-7788(02)00081-6, 2003. 25943

25 Dyer, A. J.: The turbulent transport of heat and water vapour in an unstable atmosphere, *Q. J. R. Meteorol. Soc.*, 93, 501–508, doi:10.1002/qj.49709339809, 1967. 25945

Garratt, J. R.: *The Atmospheric Boundary Layer*, Cambridge University Press, Cambridge, UK, 1992. 25945, 25946, 25949, 25950

Grimmond, C. S. B. and Oke, T. R.: Evapotranspiration rates in urban areas, *AHS Publ.*, 259, 235–243, 1999. 25943

30 Grimmond, C. S. B., Oke, T. R., and Timothy, R.: Heat storage in urban areas: local-scale observations and evaluation of a simple model, *J. Appl. Meteor.*, 38, 922–940, doi:10.1175/1520-0450(1999)038<0922:HSIUAL>2.0.CO;2, 1999. 25943

The diurnal evolution of the urban heat island of Paris

H. Wouters et al.

[Title Page](#)[Abstract](#)[Introduction](#)[Conclusions](#)[References](#)[Tables](#)[Figures](#)[◀](#)[▶](#)[◀](#)[▶](#)[Back](#)[Close](#)[Full Screen / Esc](#)[Printer-friendly Version](#)[Interactive Discussion](#)

The diurnal evolution of the urban heat island of Paris

H. Wouters et al.

[Title Page](#)

[Abstract](#)

[Introduction](#)

[Conclusions](#)

[References](#)

[Tables](#)

[Figures](#)

[◀](#)

[▶](#)

[◀](#)

[▶](#)

[Back](#)

[Close](#)

[Full Screen / Esc](#)

[Printer-friendly Version](#)

[Interactive Discussion](#)



Oleson, K. W., Bonan, G. B., Feddema, J., and Jackson, T.: An examination of urban heat island characteristics in a global climate model, *Int. J. Climatol.*, 31, 1848–1865, doi:10.1002/joc.2201, 2011. 25953

5 Press, W. H., Teukolsky, S. A., Vetterling, W. T., and Flannery, B. P.: *Numerical Recipes in FORTRAN: the Art of Scientific Computing*, 2nd edn., Cambridge University Press, Cambridge, 1992. 25945

10 Rodell, M., Houser, P. R., Jambor, U., Gottschalck, J., Mitchell, K., Meng, C.-J., Arsenault, K., Cosgrove, B., Radakovich, J., Bosilovich, M., Entin, J. K., Walker, J. P., Lohmann, D., and Toll, D.: The global land data assimilation system, *B. Am. Meteorol. Soc.*, 85, 381–394, doi:10.1175/BAMS-85-3-381, 2004. 25946

Sarkar, A. and De Ridder, K.: The urban heat island intensity of Paris: a case study based on a simple urban surface parametrization, *Bound.-Layer Meteorol.*, 138, 511–520, doi:10.1007/s10546-010-9568-y, 2010. 25947

15 Smargiassi, A., Goldberg, M. S., Plante, C., Fournier, M., Baudouin, Y., and Kosatsky, T.: Variation of daily warm season mortality as a function of micro-urban heat islands., *J. Epidemiol. Commun. Health*, 63, 659–64, doi:10.1136/jech.2008.078147, 2009. 25943

Sugawara, H. and Narita, K.: Roughness length for heat over an urban canopy, *Theor. Appl. Climatol.*, 95, 291–299, 2008. 25953

20 Taha, H.: Urban climates and heat islands: albedo, evapotranspiration, and anthropogenic heat, *Energy Build.*, 25, 99–103, doi:10.1016/S0378-7788(96)00999-1, 1997. 25943

Taha, H., Akbari, H., Rosenfeld, A., and Huang, J.: Residential cooling loads and the urban heat island – the effects of albedo, *Build. Environ.*, 23, 271–283, doi:10.1016/0360-1323(88)90033-9, 1988. 25943

25 Van Weverberg, K., De Ridder, K., and Van Rompaey, A.: Modeling the contribution of the Brussels heat island to a long temperature time series, *J. Appl. Meteor. Climatol.*, 47, 976–990, doi:10.1175/2007JAMC1482.1, 2008. 25948, 25953

Wittich, K.-P. and Hansing, O.: Area-averaged vegetative cover fraction estimated from satellite data, *Int. J. Biometeorol.*, 38, 209–215, doi:10.1007/BF01245391, 1995. 25947

30 Xue, M., Droege, K. K., and Wong, V.: The Advanced Regional Prediction System (ARPS) – a multi-scale nonhydrostatic atmospheric simulation and prediction model. Part I: Model dynamics and verification, *Meteorol. Atmos. Phys.*, 75, 161–193, doi:10.1007/s007030070003, 2000. 25944, 25945

The diurnal evolution
of the urban heat
island of Paris

H. Wouters et al.

[Title Page](#)

[Abstract](#)

[Introduction](#)

[Conclusions](#)

[References](#)

[Tables](#)

[Figures](#)

◀

▶

◀

▶

[Back](#)

[Close](#)

[Full Screen / Esc](#)

[Printer-friendly Version](#)

[Interactive Discussion](#)



Xue, M., Droege, K. K., Wong, V., Shapiro, A., Brewster, K., Carr, F., Weber, D., Liu, Y., and Wang, D.: The Advanced Regional Prediction System (ARPS) – a multi-scale nonhydrostatic atmospheric simulation and prediction tool. Part II: Model physics and applications, *Meteorol. Atmos. Phys.*, 76, 143–165, doi:10.1007/s007030170027, 2001. 25944, 25945

5 Zilitinkevich, S., Fedorovich, E., and Shabalova, M.: Numerical model of a non-steady atmospheric planetary boundary layer, based on similarity theory, *Bound.-Lay. Meteorol.*, 59, 387–411, doi:10.1007/BF02215460, 1992. 25946

ACPD

12, 25941–25981, 2012

The diurnal evolution of the urban heat island of Paris

H. Wouters et al.

[Title Page](#)

[Abstract](#)

[Introduction](#)

[Conclusions](#)

[References](#)

[Tables](#)

[Figures](#)

◀

▶

◀

▶

[Back](#)

[Close](#)

[Full Screen / Esc](#)

[Printer-friendly Version](#)

[Interactive Discussion](#)



The diurnal evolution of the urban heat island of Paris

H. Wouters et al.

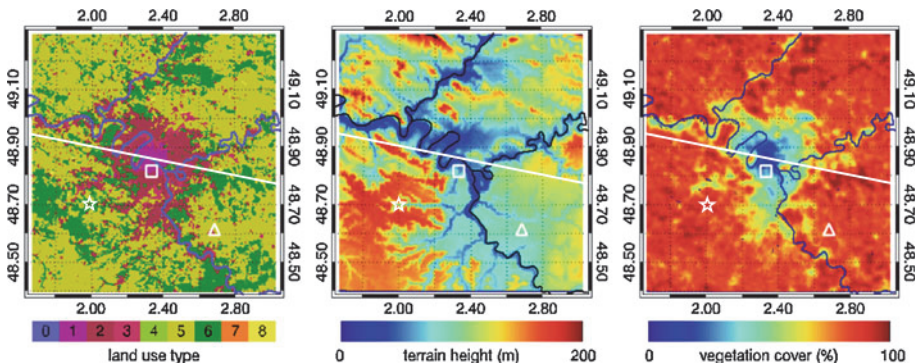


Fig. 1. Paris 1-km simulation domain showing land-use type at the left. The different land-use types are defined as water (0), urban (1), sub-urban (2), industrial (3), grass (4), crops (5), forest (6), snow/ice (7), shrubs (8). The rectangular and the triangular box represent the locations of the urban (Paris-Montsouris, square) and rural (Melun, triangle) stations, respectively. The star indicates the location of the radio soundings at Trappes. The line indicates the vertical transect along the prevailing east wind in the base run used for the vertical temperature profile analysis through the city. The map in the middle shows terrain height, and that at the right shows percentage vegetation cover. The coordinates shown on the sides are in decimal degrees longitude and latitude.

[Title Page](#)

[Abstract](#)

[Introduction](#)

[Conclusions](#)

[References](#)

[Tables](#)

[Figures](#)

◀

▶

◀

▶

[Back](#)

[Close](#)

[Full Screen / Esc](#)

[Printer-friendly Version](#)

[Interactive Discussion](#)

The diurnal evolution of the urban heat island of Paris

H. Wouters et al.

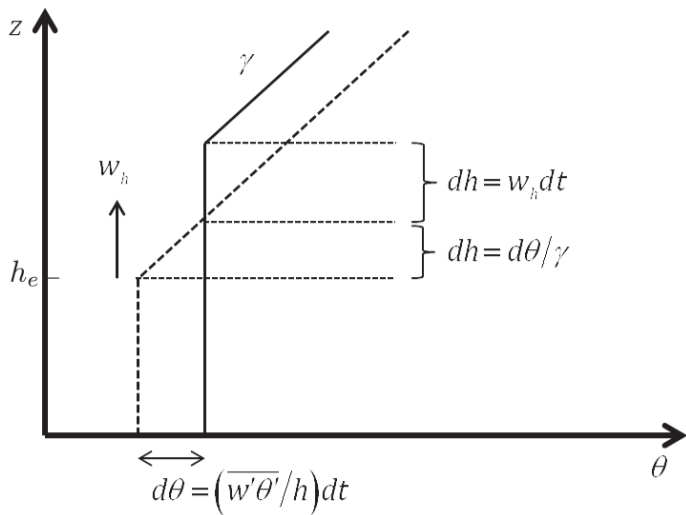


Fig. 2. The evolution of the potential temperature profiles accounting for the effect of vertical velocity w_h for the CBL. The thick dashed line depicts the situation at time t , and the full lines the situation at a time step dt later.

Title Page	
Abstract	Introduction
Conclusions	References
Tables	Figures
◀	▶
◀	▶
Back	Close
Full Screen / Esc	
Printer-friendly Version	
Interactive Discussion	

The diurnal evolution of the urban heat island of Paris

H. Wouters et al.

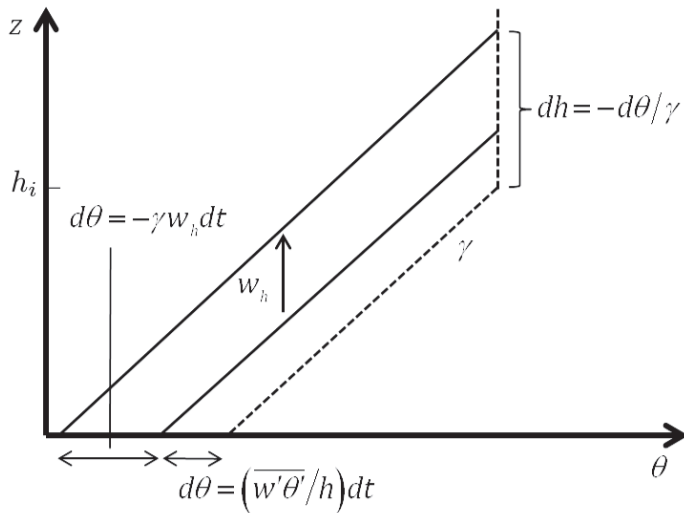


Fig. 3. Idem to Fig. 2, but for the NBL.

Title Page	
Abstract	Introduction
Conclusions	References
Tables	Figures
◀	▶
◀	▶
Back	Close
Full Screen / Esc	
Printer-friendly Version	
Interactive Discussion	

The diurnal evolution of the urban heat island of Paris

H. Wouters et al.

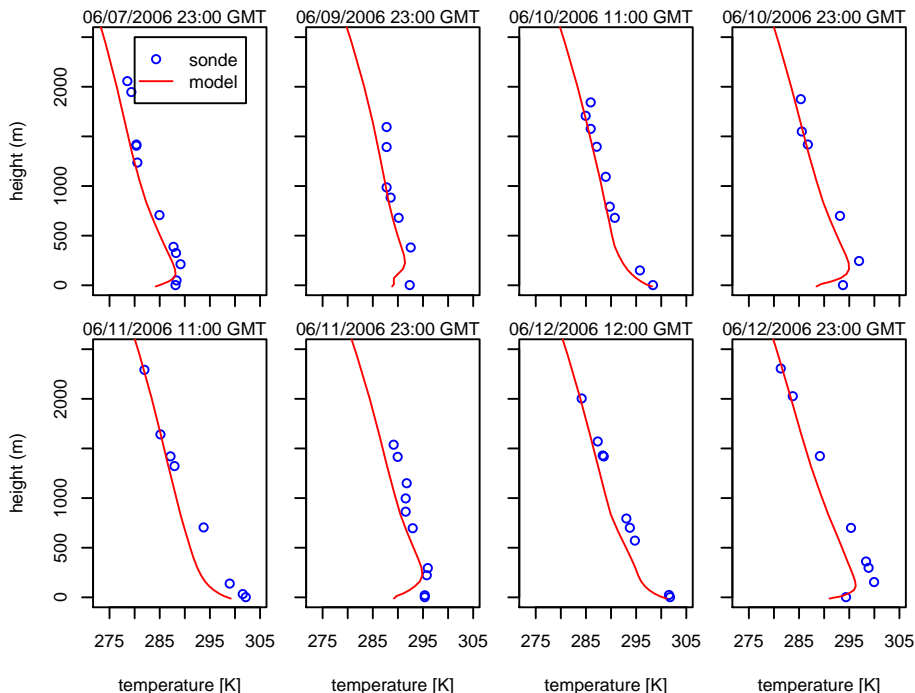


Fig. 4. Comparison between radio soundings and model output (base run) at Trappes during the selected 5-day period of clear-sky conditions.

[Title Page](#)

[Abstract](#)

[Introduction](#)

[Conclusions](#)

[References](#)

[Tables](#)

[Figures](#)

[◀](#)

[▶](#)

[◀](#)

[▶](#)

[Back](#)

[Close](#)

[Full Screen / Esc](#)

[Printer-friendly Version](#)

[Interactive Discussion](#)

The diurnal evolution of the urban heat island of Paris

H. Wouters et al.

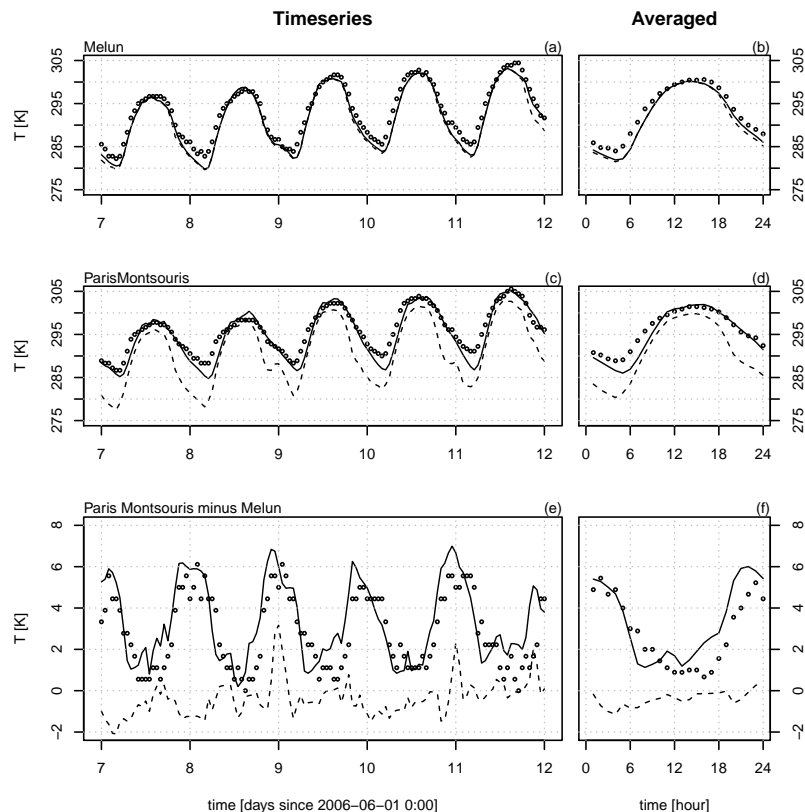


Fig. 5. The temperature time series for Melun (a), Paris-Montsouris (c), and the difference between the sites (e), for the observations (circles), base run (full line) and scenario run (dashed line) between 7 June 2006 00:00 UTC and 12 June 2006 00:00 UTC, and their hourly averaged diurnal cycle (b, d, f).

[Title Page](#)

[Abstract](#)

[Introduction](#)

[Conclusions](#)

[References](#)

[Tables](#)

[Figures](#)

[◀](#)

[▶](#)

[◀](#)

[▶](#)

[Back](#)

[Close](#)

[Full Screen / Esc](#)

[Printer-friendly Version](#)

[Interactive Discussion](#)

The diurnal evolution of the urban heat island of Paris

H. Wouters et al.

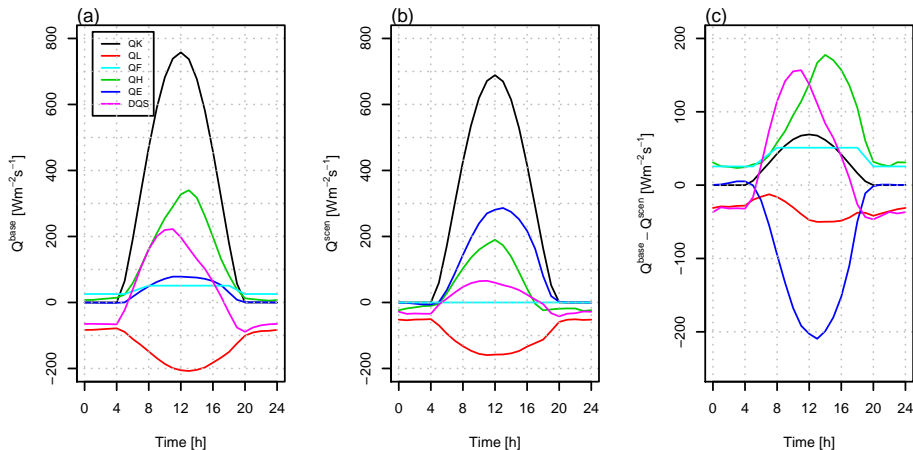


Fig. 6. The diurnal cycle averaged over the selected 5-day period is shown for net shortwave radiation (Q_K), net long-wave radiation (Q_L), anthropogenic heat (Q_F), sensible heat (Q_H), latent heat (Q_E) and de storage heat (ΔQ_S). **(a)** shows the fluxes at Paris-Montsouris (city centre) for the base run, **(b)** those for the scenario run and **(c)** the difference between the two.

[Title Page](#)

[Abstract](#)

[Introduction](#)

[Conclusions](#)

[References](#)

[Tables](#)

[Figures](#)

◀

▶

◀

▶

[Back](#)

[Close](#)

[Full Screen / Esc](#)

[Printer-friendly Version](#)

[Interactive Discussion](#)

The diurnal evolution of the urban heat island of Paris

H. Wouters et al.

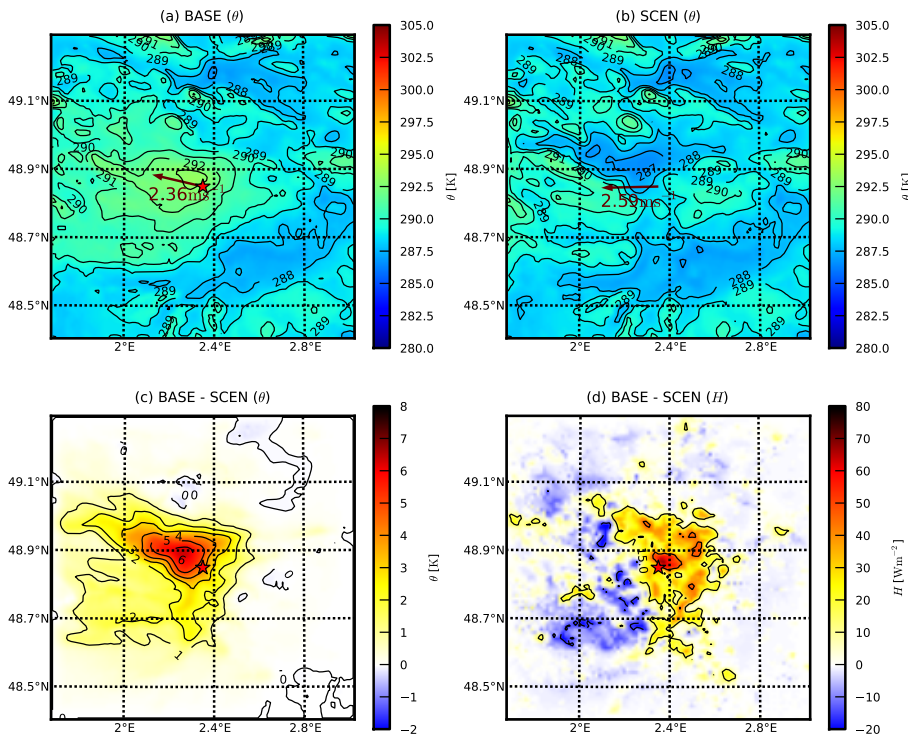


Fig. 7. The potential temperature in K over Paris for the base run **(a)** and scenario run **(b)** at 23:00 UTC at the lowest model layer above the surface (at a height of 12.5 m). **(c)** shows the difference between **(a)** and **(b)**. the difference in sensible heat (in W m^{-2}) is given by **(d)**. between the base run and scenario run. The city centre is indicated with a red star. The horizontal wind vector at 12.5 m above the surface at the city centre is shown for the base and scenario run.

The diurnal evolution of the urban heat island of Paris

H. Wouters et al.

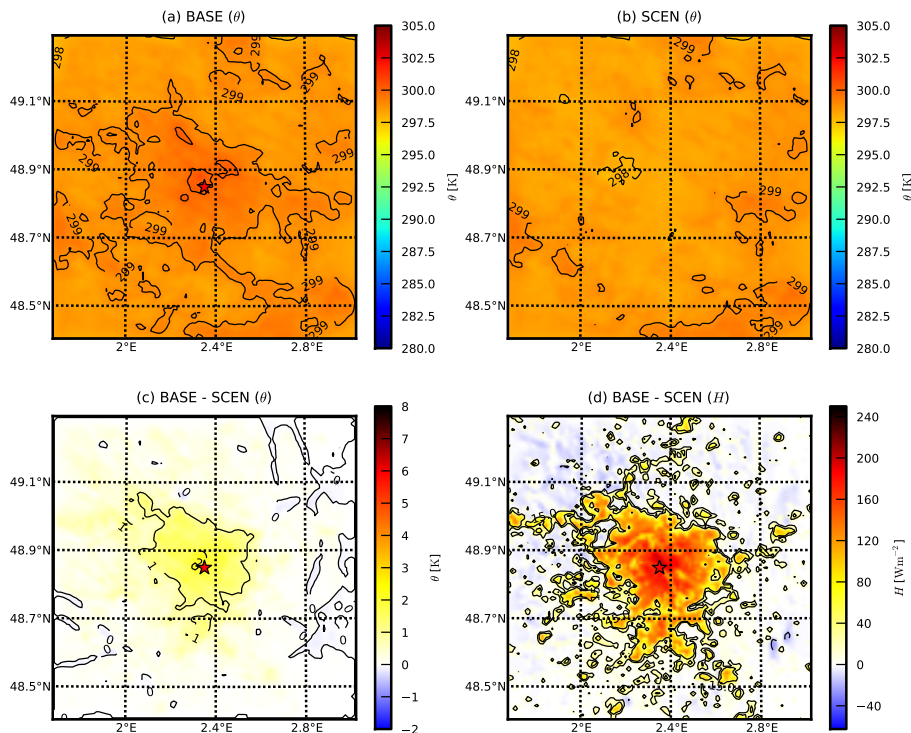


Fig. 8. Idem to Fig. 7, but for 15:00 UTC.

The diurnal evolution of the urban heat island of Paris

H. Wouters et al.

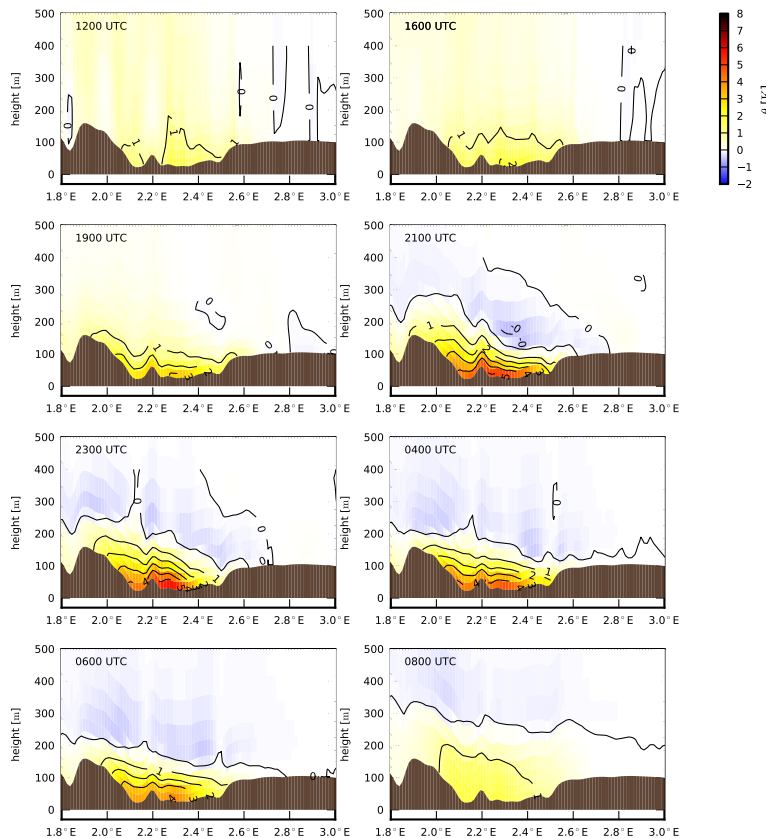


Fig. 9. The diurnal cycle of vertical profile of potential temperature difference in K between the base run and scenario run. Each panel represents the averaged profile for the specified hour over the selected 5-day period. The profiles are taken in the west-east direction through centre of Paris.

[Title Page](#)

[Abstract](#)

[Introduction](#)

[Conclusions](#)

[References](#)

[Tables](#)

[Figures](#)

[◀](#)

[▶](#)

[◀](#)

[▶](#)

[Back](#)

[Close](#)

[Full Screen / Esc](#)

[Printer-friendly Version](#)

[Interactive Discussion](#)

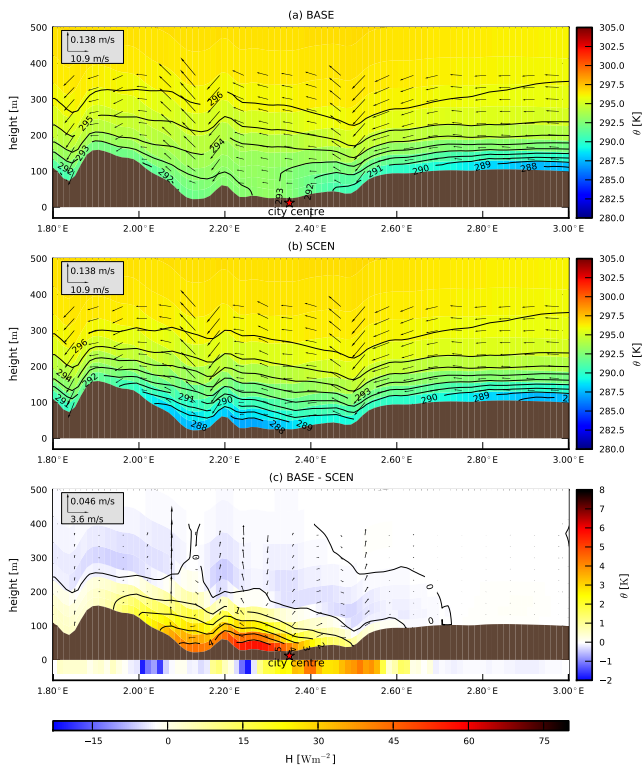


Fig. 10. (a) and (b) show the vertical profile of potential temperature in K over Paris at 23:00 UTC averaged for the 5-day period for the base run and scenario run, respectively. The profiles are taken in the west-east direction through the centre of Paris. The lower (c) shows the difference between (a) and (b). All panels are stretched in the vertical by a factor of 130 including the wind arrows. The difference in surface flux between the base run and scenario run is added at the bottom of (c).

**The diurnal evolution
of the urban heat
island of Paris**

H. Wouters et al.

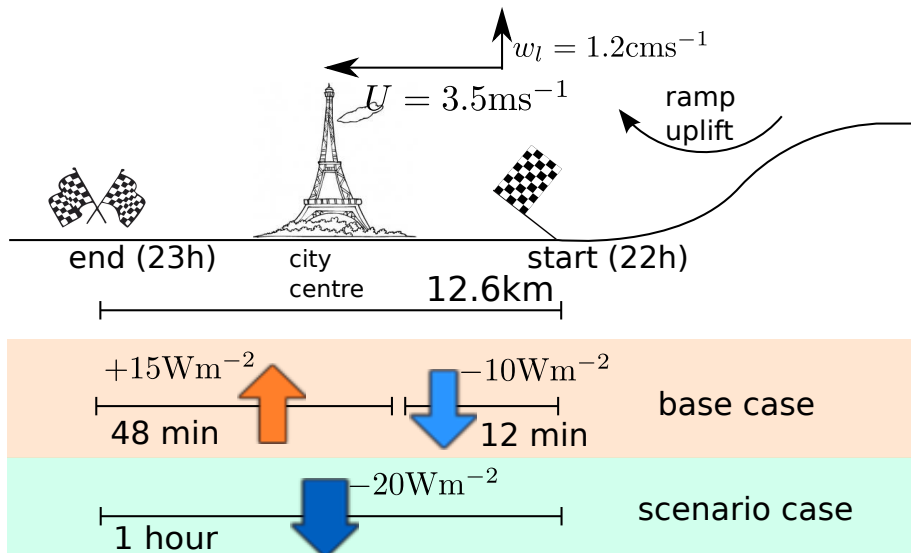


Fig. 11. Overview of the idealized advection model setup over Paris for the base case and the scenario case. Surface sensible heat fluxes, horizontal and vertical wind speed and duration of simulation are shown.

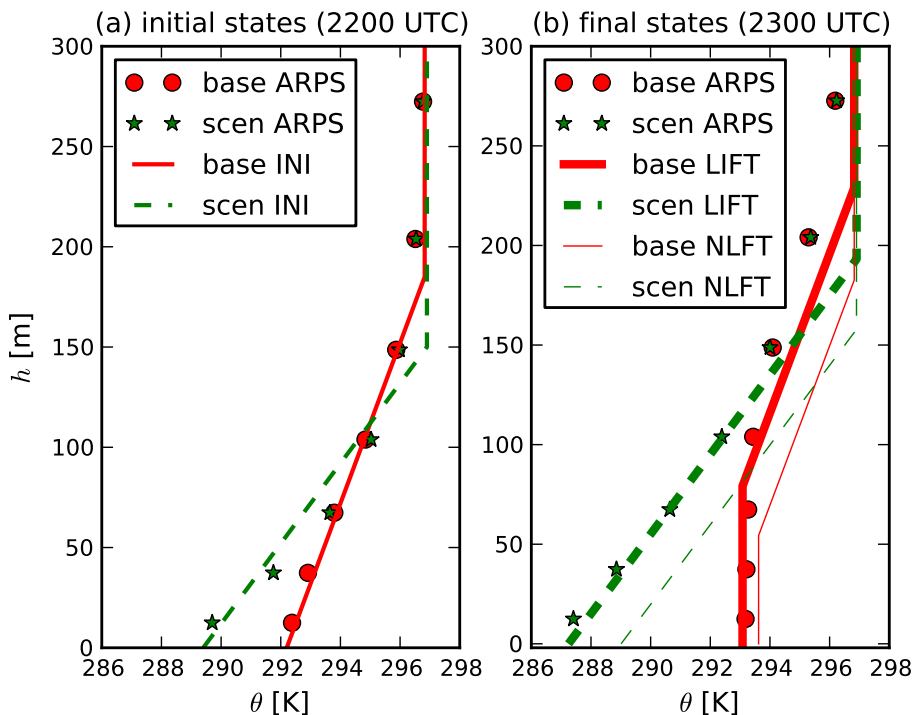


Fig. 12. Vertical potential temperature profiles from ARPS and from idealized boundary-layer advection models. h indicates the height above ground level. The initial (22:00 UTC) and final (23:00 UTC) states are plotted on **(a)** and **(b)**, respectively. In both panels, the profiles from the ARPS output are indicated with red circles and green stars for the base run and scenario run, respectively. The full red line in **(a)** represents the fitted initial state for the idealized advection models for the base case (base INI), and the dashed green line that for the scenario case (scen INI). In **(b)**, thick lines are referring to the final states of the idealized models with orographic uplift (LIFT), and thin lines without orographic uplift (NLFT) for the respective scenarios.

The diurnal evolution of the urban heat island of Paris

H. Wouters et al.

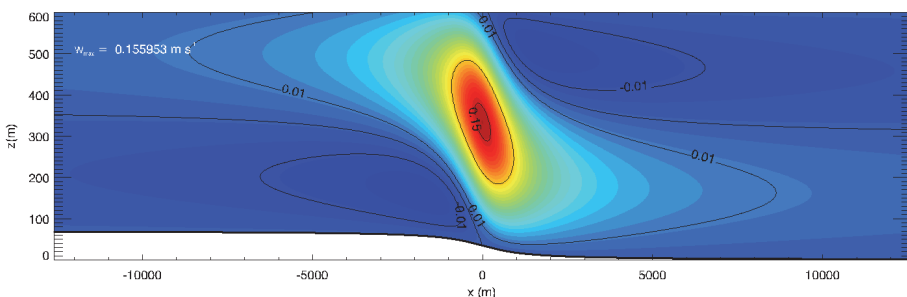


Fig. A1. Vertical velocity relative to the slope-following wind induced by a ramp in a stably stratified flow for a vertical atmospheric slice.

Title Page

Abstract

Introduction

Conclusion

References

Tables

Figures

1

▶

Back

Close

Full Screen / Esc

[Printer friendly Version](#)

Interactive Discussion